Egypt. J. Chem. **Vol. 67**, No. 7 pp. 377 - 387 (2024)

Egyptian Journal of Chemistry

http://ejchem.journals.ekb.eg/

Fabrication of a Green Nanocomposite Film-Based Polylactic Acid Loaded Cellulose Acetate- Ag Nanoparticles - Curcumin Nanoparticles For Enhanced Antibacterial Activities

Dina F. Katowah[a]*, Bdor A Almalki[a]

[a]*Department of Chemistry, Faculty of Applied Science, Umm Al-Qura University, P.O. Box 16722, Makkah, 21955, Saudi Arabia*

Abstract

Nowadays, there is a growing concern regarding the conservation of ecological systems. The continuous usage of polymers greatly contributes to environmental pollution. Consequently, the development to eliminate environmental pollution. Therefore, the use of locally sourced biomaterials in polymer composites promotes environmental awareness, reduces reliance on unsustainable synthetic materials, and has the advantage of lower cost of natural fibers compared to synthetic alternatives. The key objective of this research is to establish an environmentally friendly nanocomposite (NCs) film by utilizing natural resources. To achieve this, the polylactic acid-cellulose acetate-curcumin-silver (PLA-CA-CUR-Ag) NCs film was synthesized in four steps using a simple solution-casting and ultrasonic irradiation. Acetylation of cellulose (CE) extracted from sukkari palm leaf using acetic anhydride, AcOH and H_2SO_4 catalyst. Additionally, CUR was transformed into nanoparticles (NPs) using physico-chemical fabrication techniques. Ag NPs were synthesized using the solid-state approach, utilizing the pomegranate peel. These NPs and CA were distributed in PLA as the supporting matrix. The structure of the novel synthesized NCs film was proved by several tools as FT-IR, XRD, UV, SEM, TGA, and DTG. In addition to revealing the importance of synthesized NCs film, as they have proven antibacterial and antifungal effectiveness. CA, CUR NPs, and Ag NPs increased the activity of PLA against Bacillus subtilis and Candida albicans, whereas PLA alone did not show any activity.

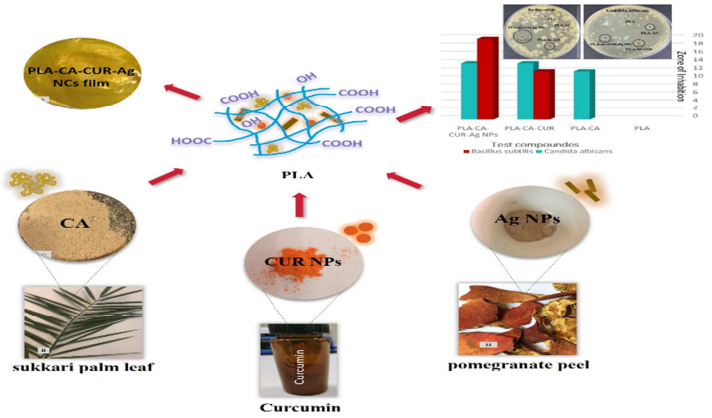

Keywords: Sukkari palm leaf; Curcumin NPs; Pomegranate peel; cellulose; Polylactic acid; PLA-CA-CUR-Ag NCs; Films

*Corresponding author e-mail: Correspondence author: Dina F. Katowah(dfkatoaah@hotmail.com, dfkatoaah@uqu.edu.sa)
EJCHEM use only: Received date 10 October 2023; revised date 17 December 2023; accepted date 07 January 2024
DOI: 10.21608/EJCHEM.2024.236051.8726

1. Introduction

CA, an alternative biopolymer, possesses both antimicrobial properties and mechanical strength. It is produced by converting CE into a derivative through a chemical reaction involving acetic anhydride and acetic acid, with sulfuric acid serving as a catalyst [1]. CA is an important ester of CE [2] and has gained increasing attention due to its advantageous characteristics, including biocompatibility, biodegradability, favorable mechanical properties, insolubility in water, high affinity, non-toxicity, good hydrolytic stability, excellent chemical resistance, and relatively low cost. Moreover, CA has potential applications in various fields, such as wound dressing, filament-forming matrices, antimicrobial membranes, affinity membranes, biomedical separation, and biomedical NCs [3]. Numerous articles have focused on the recent advancements in antimicrobial additives for CA, covering aspects such as their preparation, biocidal action, and application [3-8].

CUR, a polyphenolic compound, has garnered significant attention in global studies due to its diverse biological activities [9-13]. It is derived from turmeric, an ancient spice commonly used in Asian traditional remedies [14]. CUR has antimicrobial properties that include antifungal, antibacterial, antiviral, and antimalarial activity. Notably, CUR has demonstrated extensive antibacterial efficacy and has been deemed safe even at large doses (up to 12 g per day) based on clinical human trials. This safety profile has prompted the synthesis of various CUR derivatives to create antimicrobial drugs with modified and enhanced antibacterial activities [15, 16]. CUR and other antimicrobial derivatives have been combined to produce antimicrobial gels and emulsions for skin that improve skin protection and wound treatment capabilities[17]. Furthermore, CUR has been incorporated with hydrogel Ag NPs to enhance the functionality of hydrogel Ag NCs as targeted agents for wound dressing and antimicrobial applications [17]. Since CUR exhibits poor solubility and low absorption, it is often utilized in NPs form, which offers advantages such as improved solubility and absorption [18].

Ag NPs, being a fascinating material, have attracted significant attention in research and development aimed at enhancing their inherent properties [19, 20]. This noble nanometal is renowned for its antimicrobial capabilities, which find relevance in various applications such as orthopedics [21], packaging [22], medical devices [23], footwear, and household items [24]. Moreover, Ag NPs possess unique properties that make them highly promising in diverse fields including electronics [25], photonics [26], photocatalysis [27], surface-enhanced Raman spectroscopy detection [28], biosensor materials [29], etc.

PLA is a thermoplastic polymer known for its non-toxicity, biodegradability, and excellent mechanical properties. It finds applications in various fields such as agriculture, packaging, engineering materials, and medical textile preparation [30, 31]. Additionally, PLA is biocompatible with body fluids, and its degradation products do not cause any local or systemic toxic effects [32]. Therefore, incorporating antimicrobial additives into PLA is an advantageous approach to addressing microbial proliferation [33]. In response to the growing demand for eco-friendly resources, scientists have been focusing on developing materials derived from nature [34, 35].

Currently, there is a growing concern regarding the conservation of ecological systems. Most synthetic polymers, however, are derived from petrochemicals and possess limited biodegradability. The continuous usage of polymers greatly contributes to environmental pollution. Recently, traditional materials made from synthetic composites, which contribute to greenhouse gas emissions, have been replaced with environmentally friendly and renewable composite materials [36]. Consequently, the development of environmentally friendly materials utilizing natural resources has emerged as a significant challenge over the past decade. Additionally, the utilization of locally sourced bio-materials in polymer composites promotes environmental awareness, reduces reliance on unsustainable synthetic materials, and offers a cost advantage due to the lower cost of natural fibers compared to synthetic alternatives [37].

The hybrid of natural polymers with Ag NPs in NCs film will have several industrial applications as sensors which can be used to detect factors that endanger human life, such as heavy metal contamination of drinking water and the detection of toxic fumes and gases in factories or laboratories [29,34]. Also, NCs film used in manufacturing the energy device as lithium ion batteries, supercapacitors, and solar cells [25,26].

Given the aforementioned information, researchers have shown significant interest in the development of eco-friendly green NCs. In this study, a novel green NCs film was created by combining CA, CUR NPs, and Ag NPs with PLA matrix. The synthesis of the film NCs involved a straightforward four-step process, including solution casting and ultrasonic irradiation. Firstly, CE was extracted from sukkari palm leaves and acetylated through a reaction involving acetic anhydride (Ac_2O), acetic acid (AcOH), and sulfuric acid (H_2SO_4) as the catalyst is employed. Secondly, CUR was fabricated as NPs through a physico-chemical method. Thirdly, a solid-state approach utilizing pomegranate peel was

employed to synthesize Ag NPs, which were then dispersed within the obtained CA. These NCs combine the unique advantages of each component, resulting in enhanced properties of the NCs film. Subsequently, the newly developed NCs film was subjected to testing for its antimicrobial and antifungal properties.

2. Experimental Methodology

2.1. Materials

The palm branches utilized in this study were sourced from a farm situated in Mecca, Saudi Arabia. The specific palm type used was Sukkari. The polylactic acid (PLA) material, with a thickness of 3mm, was sourced from Goodfellow in Cambridge, UK and was in its pure biopolymer form. The following chemicals and reagents were employed without purification: curcumin (CUR) with a purity of 98%, glacial acetic acid, acetic anhydride, sulfuric acid, and dichloromethane, all obtained from Sigma Aldrich in the USA. Chloroform was acquired from Fisher Scientific located on Bishop Meadow Road in Loughborough, UK, while silver nitrate was obtained from Carlo Erba in Milan, Italy. Throughout the experiments, distilled water was used.

2.2. Measurements and characterization

The film morphologies have been studied in this investigation using a field-emitting scanning electron microscopy (SEM) instrument, specifically the Thermo Scientific Scios2 DualBeam System. This analysis aimed to provide fundamental information regarding the crystallographic and structural characteristics of the polymer films. Additionally, the crystallinity of the films was evaluated using XRD (X-ray diffraction) analysis. using the Rigaku Corporation model (RIGAKU ULTIMA_IV). Furthermore, TGA and differential thermogravimetry (DTG) were used to evaluate the thermal stability of the films. The TGA and DTG tests were performed using a Shimadzu DTA-60 and TGA-60 system at a heating rate of 10 °C/min under ambient atmospheric conditions. This analysis yielded information about the temperature at which the films started to degrade. To obtain information about the functional groups present in the samples and to record the Fourier Transform Infrared (FTIR) spectra, the Shimadzu FTIR - IR Affinity1S and IRSpirit spectrometer with the QATR-S accessory installed were utilized. The FTIR measurements were conducted within the 4000-300 cm−1 range. Additionally, absorption studies were conducted using Thermo Scientific Evolution 201/220 UV-Visible Spectrophotometers to investigate the absorption properties of the films.

2.3. Isolation of CE from Palm Branch

The palm leaves (Fig.1a) were first washed and dried. They were then chopped into uniform pieces with dimensions of approximately 5 x 10 cm. Subsequently, the palm leaves underwent a treatment with 3% NaOH solution as described by reference [38]: 9 g of palm leaf samples have been placed in a 500 mL round flask including 150 mL of 3% NaOH solution to begin the treatment. The flask was subsequently subjected to Reflux. at 110 °C with continuous magnetic stirring for a duration of 3 hours (Fig.1b). After the reflux process, the solid material was filtered and rinsed multiple times with distilled H2O. Subsequently, for 1.5 hours, the filtered substance was dried in a 70 °C oven. The resulting pretreated palm leaf sample is shown in Fig.1c.

2.4. Acetylation of CE

To prepare the CA, acetylation of the pretreated palm leaf sample was carried out using the following method as described in reference [41]:

Acetylation was performed using acetic anhydride as the acetylating agent, glacial acetic acid was used as the solvent, and sulfuric acid served as the catalyst. In the acetylation process, 3.5 g of the pretreated palm leaf sample was dissolved in a combined mixture consisting of 16.5 ml of AcOH, 10 ml of Ac_2O, and 1 ml of H_2SO_4. The resulting mixture was stirred using a magnetic stirrer for a duration of 5 hours at a temperature of 7 °C in an ice bath. After the reaction of acetylation, the resulting material was filtered and subjected to multiple washes using warm distilled water at a temperature of 40 °C. Subsequently, the filtered substance was dried in an oven set at 70 °C for a duration of 1.5 hours. The CA obtained from this process is shown in Fig.1d.

2.5. Synthesis of CUR NPs

As mentioned in the literature [18, 40], the preparation of (CUR NPs) was achieved through a physico-chemical fabrication method. The following procedure was followed: Firstly, to prepare a CUR solution, 0.1 g of CUR was mixed with 20 ml of dichloromethane (Fig. 1e). From this solution, 1 ml was added drop by drop into 50 ml of boiling water using a burette. The mixture was then subjected to ultrasonication for 30 minutes at a frequency of 50 kHz. After ultrasonication, the solution was subjected for stirring about 20 minutes at 800 rpm, as a result, a clear orange-colored precipitate formed. (Fig. 1f, g). Subsequently, the solution was then centrifuged for separating the resulting precipitate from the supernatant. The supernatant was discarded, and the remaining pellet (Fig. 1g) was obtained. Finally, the obtained pellet was oven-dried to obtain the desired (CUR NPs) (Fig. 1h).

2.6. Synthesis of Ag NPs

The pomegranate fruits (Fig. 1i) were first washed using distilled water and then sliced. Subsequently, the peel was left to dry at room temperature for a period of 7 days (Fig. 1j). Next, the dried pomegranate peel was ground. The preparation of (Ag NPs) was carried out utilizing a solid-state

method [19]. During this procedure, 2 grams of finely ground pomegranate peel were combined with 0.3 grams of AgNO3 and thoroughly mixed (Fig. 1k). The resulting powders were subsequently placed in a furnace and subjected to 600 °C temperature for a duration of 3 hours. The formation of Ag NPs is illustrated in Fig. 1(i-l).

Figure 1: Isolation of cellulose acetate from Palm Branch (a-c), cellulose Acetate (d), Synthesis of nano CUR (e-h), Synthesis of Ag NPs (i-l)

2.7. Preparation of PLA-CA-CUR-Ag NCs film

The PLA-CA-CUR-Ag NCs film was fabricated using a solution-casting and ultrasonic irradiation method based on a previously reported procedure with some modifications [40]. To begin, PLA was added to chloroform and stirred at room temperature for 12 hours until it completely dissolved. Afterward, CA was introduced into the PLA solution and stirred for an additional 6 hours. The CUR NPs were then mixed with the PLA-CA mixture and stirred for 3 hours, followed by sonication for 1 hour. Separately, Ag NPs were added to chloroform and sonicated for 30 minutes. Subsequently, the obtained Ag NPs solution was added to the PLA solution and subjected to sonication for a duration of 1 hour to enhance the dispersion of CA, CUR, and Ag NPs. Then, the solution was poured into a Petri dish, and the process of preparing the PLA-CA-CUR-Ag NCs film is depicted in Fig. 2.

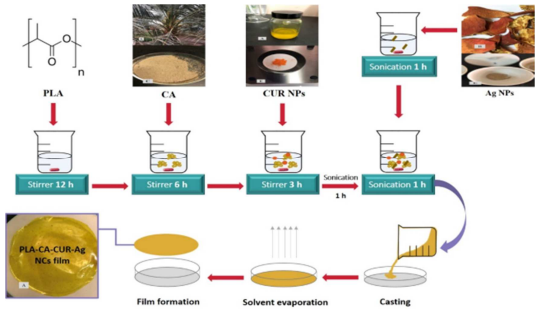

Figure 2: Preparation of PLA-CA-CUR-Ag NCs film

For comparison, the same preparation procedure was repeated three times to synthesize other films. Pure PLA film (Fig. 3a), PLA-AC film (Fig. 3b), and PLA-CA-CUR NCs film (Fig. 3c) were prepared following similar steps. The abbreviations for the fabricated films and their composition with different polymer ratios are provided in Table 1.

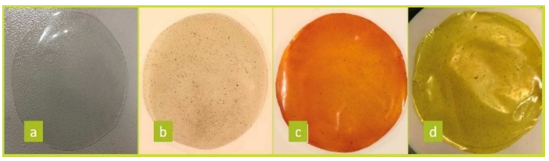

Figure 3: Pure PLA (a), PLA-AC (b), PLA-CA-CUR NCs (c) and PLA-CA-CUR-Ag NCs (d) films

Table 1: The abbreviations and the chemical compositions for nanocomposites polymer film

Formulation	PLA (g)	CA (g)	CUR (g)	Ag NPs (g)
PLA	1	-	-	-
PLA/CA	0.95	0.05	-	-
PLA/CA/CUR	0.94	0.05	0.01	-
PLA/CA/CUR/Ag NPs	0.93	0.05	0.01	0.01

2.8. Assessment of Antimicrobial Activity

The films' antibacterial activity was tested toward 4 bacteria and one fungus from the microbiology laboratory at the University of King Abdulaziz Hospital in Jeddah, Saudi Arabia. Gram-positive (+ve) bacteria, specifically Bacillus subtilis ATCC 6633and Staphylococcus aureus ATCC 29213, were present, as were gram-negative (-ve) bacteria, specifically Pseudomonas aeruginosa ATCC 27853 and Escherichia coli ATCC 35218. Candida albicans ATCC 76615 was the fungal strain used.

2.8.1. Inoculum preparation

On Muller-Hinton agar plates, bacterial culture collections were grown. A loopful of overnight bacterial cells from the agar plates were moved into 5 mL of regular saline (85% NaCl), and the suspension's turbidity was set to 1-5 x 106 CFU/mL. The agar diffusion approach was used to conduct preliminary antibacterial and antifungal activity screening, as described previously [41]. In this technique, Petri dishes with a diameter of 90 mm were filled with 25 mL of Muller-Hinton agar, and 1 mL of the bacterial culture (1 × 106 CFU/mL) was added to the agar medium. Each strain was inoculated individually. On the agar plates containing the seeded bacteria, 6 mm diameter wells were created. Subsequently, 50 µL of each film sample, prepared at

a concentration of 20 mg/mL, was added to the respective wells. As a negative control, DMSO was used. The Petri dishes were subsequently placed in an incubator set at 37°C and incubated for 24 hours. After incubation, the absence of bacterial growth in the area surrounding the wells indicated inhibitory activity. The inhibition-zones were recorded using a caliper to determine the extent of inhibition.

3. Rustle and discussion

Confirmation of the preparation of CA, CUR NPs, and Ag NPs was carried out using FT-IR and UV techniques. The FT-IR spectroscopy analysis was performed on the extracted CE from sukkari palm leaf and its acetylated form (Fig. 4). In the spectrum of CE, an absorption band for stretching -OH groups at ν = 3400 cm^{-1} was observed. In comparison to CA, the intensity of the -OH absorption band decreased, indicating a decrease in -OH content in the acetylated CE. This reduction confirmed the successful acetylation of CE. A shoulder peak near the stretching vibrations peak of -OH at 2924 $cm^{-1}$was refer to C-H bond stretching vibration which are present in aliphatic groups of CE. The absorption bands at ν = 1751 cm^{-1}were identified as ester carbonyl groups, the peak at 1375 cm-1 referred to the existence of C-H bonds in the acetyl group, and the absorption at 1235 $cm^{-1}$was attributed to the presence of C-O bonds in the (O-C=O group). These peaks provided confirmation of the formation of ester bonds in the acetylated CE, resulting in an increase in their relative intensity [38, 43]. Furthermore, distinctive peaks were observed, confirming the acetylation of C isolated from sukkari palm leaf.

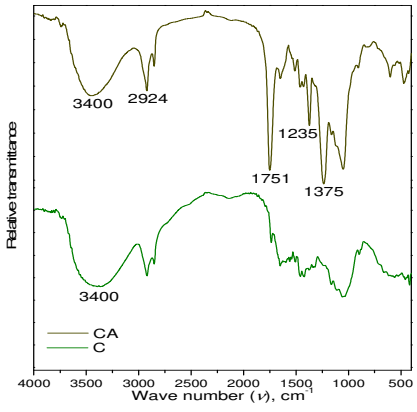

Figure 4: FT-IR of C and CA

Fig. 5a depicts the FT-IR spectrum of CUR NPs, verifying the existence of all CUR functional groups. The stretching of the C=C bond was observed at 1627 cm^{-1}, whereas the peak at 1453 cm^{-1}corresponded to the C=H bond in the CUR molecule. The stretching and vibration of C=O were represented by the absorption bands at 1610 cm-1 and 1506 cm^{-1}, respectively. Furthermore, the stretching of C-N resulted in a peak at 1037 cm^{-1}. The stretching of O-H groups was observed at 3380 cm^{-1}, while the enol peaks of C-O-C and C-O were located at 1110 $cm^{-1}$and 1272 cm^{-1}, respectively [39]. The UV spectroscopy image (Fig. 5b) of CUR NPs provided further confirmation of their presence. The unique absorption of CUR NPs has been demonstrated by the absorption peak at 419 nm [18, 39, 42].

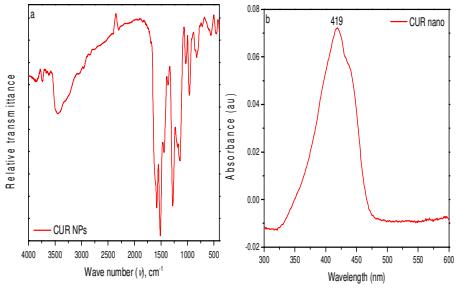

Figure 5: FT-IR (a) and UV (b) spectrum of CUR NPs

The presence of Ag NPs was also confirmed using FT-IR spectroscopy, as depicted in Fig. 6a. The spectrum exhibited peaks at 3272 cm^{-1}, which could be caused by stretching vibrations of OH groups existing in water as a result of the precursor. Furthermore, two peaks at 1043 $cm^{-1}$and 1651 cm^{-1}may be associated with bioorganic compound C-C and C=O bonds, such as residues of glucose and chains of carbons. [44-46]. The presence of -C=O symmetry stretching vibrations was observed at 1651 cm^{-1}, while the peak at 594 cm^{-1}confirmed the presence of Ag-O bonds. Furthermore, UV spectroscopy provides confirmation of the green synthesis of Ag NPs using pomegranate peel. The UV spectrum of the synthesized Ag NPs is shown in Fig. 6b, with a characteristic absorption peak observed at 414 nm. Both FT-IR and UV spectroscopy confirm the formation of Ag NPs [47].

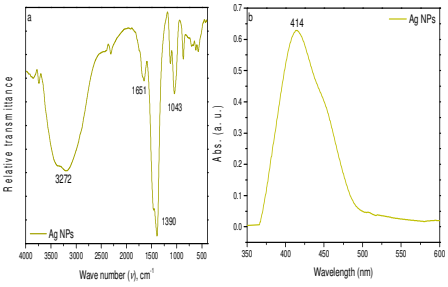

Figure 6: FTIR (a) and UV (b) spectrum of Ag NPs

The XRD diffraction patterns obtained for the films revealed of PLA, PLA-CA, PLA-CA-CUR, and PLA-CA-CUR-Ag NCs are presented in Fig. 7. In the case of PLA, it was expected to exhibit distinct X-ray diffraction peaks since it is a semi-crystalline polymer. However, these films showed a broad halo in the XRD pattern, demonstrated the amorphous nature of PLA. However, in contrast, the XRD patterns of the PLA-CA films exhibited peaks corresponding to both CA and PLA. According to previous literature [48], diffraction peaks of CA are typically observed at 2θ values around 14.7, 16.6, and 22.6 [49]. Hence, the peak at 16.6 can be attributed to CA, confirming the presence of CA in the film. Similarly, the XRD pattern of the PLA-CA-CUR NPs film displayed characteristic peaks corresponding to both PLA and CA. Furthermore, the XRD pattern showed peaks at 17.53, 18.17, and 24.54 [39], corresponding to the characteristic peaks of CUR NPs. These peaks, although appearing slightly in these NCs, are most likely attributed to the fine dispersion of a very small amount of CUR in the PLA matrix. The presence of these peaks confirms the synthesis of the PLA-CA-CUR NCs film. Moreover, the XRD pattern obtained for the PLA-CA-CUR-Ag NCs film exhibited characteristic peaks of PLA, CA, and CUR NPs, along with distinct characteristic peaks of Ag NPs at 38.13, 44.42, 64.60, and 77.52 [19]. The presence of all these peaks confirms the formation of the NCs film.

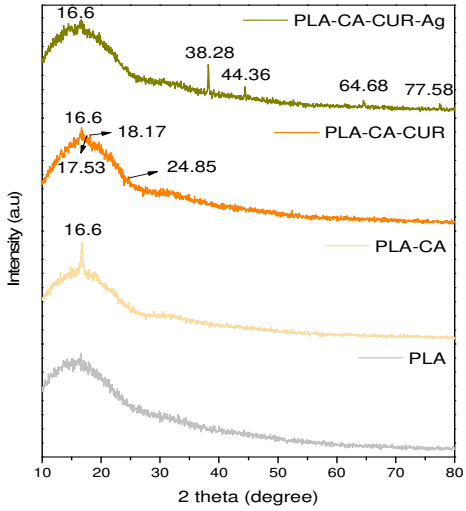

Figure 7: XRD patterns of PLA, PLA-CA, PLA-CA-CUR NCs and PLA-CA-CUR-Ag NCs films

Fig. 8 displays the FTIR spectra of the PLA film, PLA-CA film, PLA-CA-CUR NCs, and PLA-CA-CUR-Ag NCs. All of these films displayed characteristic bands at 867 cm^{-1} and 751 cm^{-1}, which are indicative of the crystalline and amorphous phases of the polymer, respectively [50]. Furthermore, at 1183 $cm^{-1}$and 1081 cm^{-1}, peaks related to the symmetric and asymmetric stretching of the complex C-O-C group were noticed. [51]. Asymmetric and symmetric CH_3 deformation vibrations have been detected at 1453 cm^{-1} and 1358 cm^{-1}, respectively [52]. The C-O stretching vibration of the ester group found in PLA molecules is responsible for the appearance of a peak at 1744 cm^{-1} [53]. Around 2933 cm^{-1}, the CH_3 stretching vibrations in saturated hydrocarbons were detected [54]. In the composite films of PLA-CA, PLA-CA-CUR, and PLA-CA-CUR-Ag, no new peaks were observed, except for minor variations in peak intensities. This indicates that there were no significant changes in the chemical structure of the PLA polymer, and no new chemical bonds were formed between PLA, CA, CUR NPs, and Ag NPs. The FTIR results suggest a physical interaction between PLA, CA, CUR NPs, and Ag NPs [51].

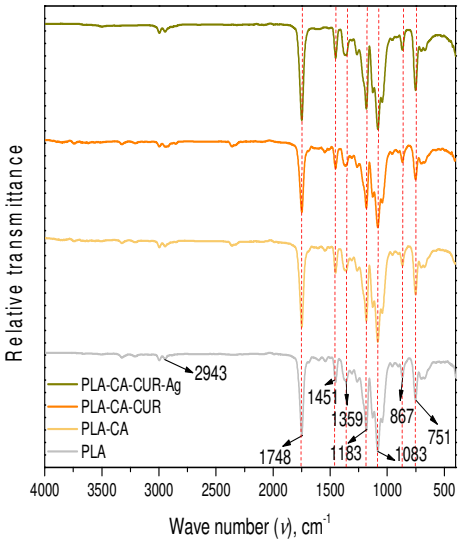

Figure 8: FT-IR spectrum of PLA, PLA-CA, PLA-CA-CUR NCs and PLA-CA-CUR-Ag NCs films

The morphology of PLA, PLA-CA, PLA-CA-CUR, and PLA-CA-CUR-Ag films was examined using SEM analysis, as depicted in Fig. 9. Pure PLA film (Fig. 9a) exhibited a smooth surface structure without any voids. The PLA-CA film (Fig. 9b) showed a uniform surface, indicating the successful combination of PLA and CA without any fractures. Similarly, the surface of the PLA-CA-CUR

film (Fig. 9c) appeared smooth and devoid of any defects. Furthermore, in the polymer matrix, the CUR NPs were evenly dispersed without agglomeration. The SEM image (Fig. 9d) reveals a smooth surface structure of the PLA-CA-CUR-Ag NCs film, with both CUR NPs and spherical Ag NPs present. The interaction between the polymer matrix and the CUR NPs as well as the Ag NPs resulted in a film with a favorable distribution of fillers, without any agglomeration. The presence of CUR and Ag NPs is responsible for the antibacterial activity exhibited by the NCs film. The CUR NPs appear as white irregular spheres spread throughout the surface.

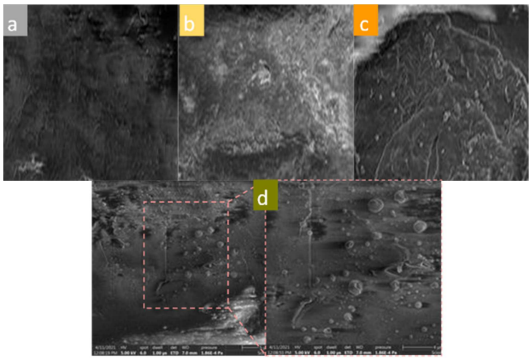

Figure 9: SEM images of PLA (a), PLA-CA (b), PLA-CA-CUR NCs (c) and PLA-CA-CUR-Ag NCs (d) films

Manufacturing NCs films were analyzed using thermogravimetric analysis (TGA-DTG) to determine thermal stability and weight loss. The TGA thermogram for PLA Fig. 10a shows two primary steps of degradation. First, the mass loss of ~7% due to the solvent evaporation remained in the film at lower temperatures. Second, weight loss of ~25% arises at 301 °C, which can be attributed to the thermal degradation of the PLA matrix. Furthermore, PLA decomposed entirely as detected at 574 °C. Parallel activity was recorded for both PLA-CA and PLA-CA-CUR matrixes, indicating that the addition of CA and CUR NPs did not alter the thermal stability of the film of PLA. However, the thermal stability of PLA is higher than PLA-CA-CUR-Ag NCs. Table 2 shows T_{10}, T_{25}, and T_{50}, representing the temperatures correlated to the decomposition of 10, 25, and 50% weight losses, respectively. Compared to other samples, PLA-CA-CUR-Ag NCs had the lowest residual mass retention and thermal stabilities. The final composite degradation temperature is CDT_{final}, where the decomposition ends [55, 56] and the maximum polymer degradation temperature PDT_{max} [57, 58] values determined for the samples (Table 2) indicate that the interactions between PLA, CA, CUR, and Ag NCs decrease the thermal stability of the PLA-CA-CUR-Ag NCs. The decreased thermal stability of PLA-CA-CUR-Ag NCs can be attributed to the strong interaction between their composites besides the dispersion quality of the nanosized filler in the polymer matrix and the amount of Ag NPs.

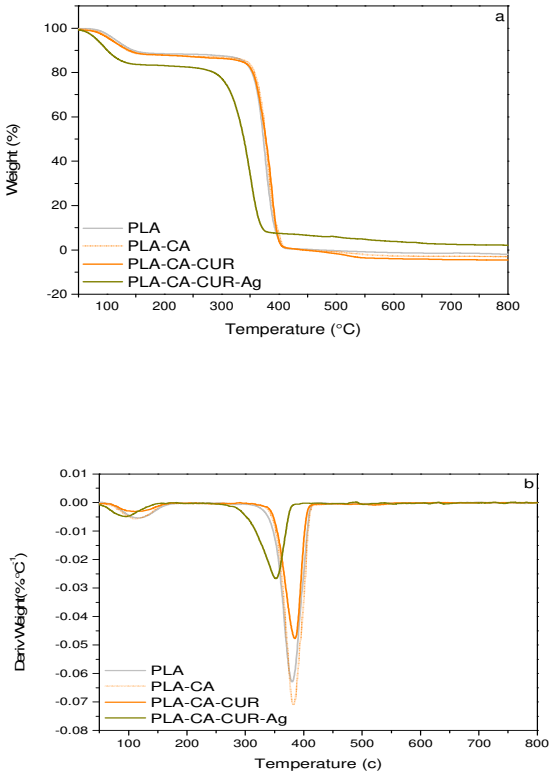

Figure 10: TGA (a) and DTG (b) curves of PLA, PLA-CA, PLA-CA-CUR NCs and PLA-CA-CUR-Ag NCs films

Table 2: Thermal behavior of PLA, PLA-CA, PLA-CA-CUR NCs and PLA-CA-CUR-Ag NCs films

	Temperature (°C) for various percentage decompositions [a]				
Sample	T_{10}	T_{25}	T_{50}	PDT_{max} [b] (°C)	CDT_{final} [a] (°C)
PLA	392	383	373	384	410
PLA-CA	398	386	377	390	410
PLA-CA-CUR	394	388	378	399	645
PLA-CA-CUR-Ag	371	355	339	357	376

[a]The values were determined by TGA at a heating rate of 10°C min^{-1}
[b]Determined from DTG curves.

4. Biological activity

To assess their antimicrobial efficacy, the four newly synthesized films were tested in vitro

against two standard strains of both gram-positive and gram-negative bacteria, as well as one fungus, as detailed in Table 3 and depicted in Figures 11 and 12. The agar diffusion assay was used as the screening method to evaluate antimicrobial activity [37]. According to the results presented in Table 3, it can be seen that the PLA film did not demonstrate any activity against the tested microbial strains. Upon analyzing the activity of the remaining three films toward bacterial resistance, it was found that the PLA-CA-CUR film displayed a moderate level of activity toward Bacillus subtilis, as evidenced by an inhibition zone diameter of 12 mm. Remarkably, the film incorporating Ag-NPs, namely PLA-CA-CUR-Ag, exhibited enhanced antibacterial activity against Bacillus subtilis, resulting in a substantial 20 mm zone of inhibition. This level of inhibition was comparable to that of the Amoxicillin/Clavulanic acid drug, which demonstrated an inhibition zone of 21.5 mm. On the other hand, when evaluating the films' antifungal activity, it was observed that three films, namely CA, CUR NPs, and Ag NPs, displayed a moderate level of activity against Candida albicans. The inhibition zone diameters were measured at 12 mm, 14 mm, and 14 mm, respectively.

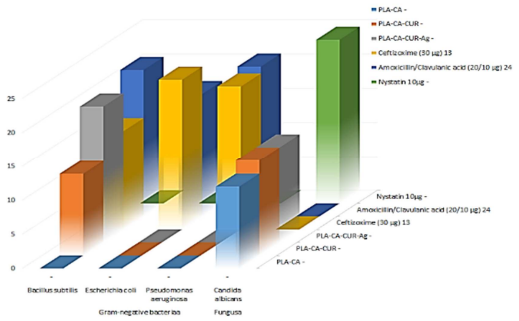

Figure 11: Antimicrobial activity of tested PLA and its NCs

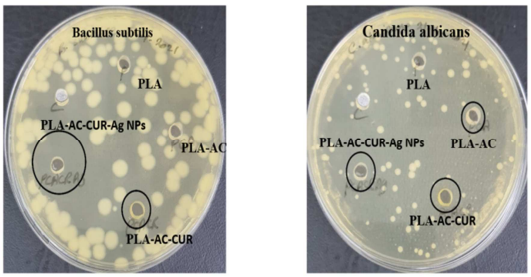

Figure 12: The activity of tested PLA and its NCs against Bacillus subtilis and Candida albicans

Table 3: Antibacterial and antifungal activities of films studied

No.	Zone diameter (mm)				
	Gram-positive bacteria[a]		**Gram-negative bacteria**[a]		**Fungus**[a]
	Staphylococcus aureus	*Bacillus subtilis*	*Escherichia coli*	*Pseudomonas aeruginosa*	*Candida albicans*
PLA	-	-	-	-	-
PLA-CA	-	-	-	-	12
PLA-CA-CUR	-	12	-	-	14
PLA-CA-CUR-Ag	-	20	-	-	14
Ceftizoxime (30 µg)	**13**	**14.5**	**22**	**21**	**-**
Amoxicillin/Clavulanic acid (20/10 µg)	**24**	**21.5**	**18**	**22**	**-**
Nystatin 10µg	**-**	**-**	**-**	**-**	**24**

[a] Reference controls for the Gram-positive and Gram-negative bacteria is "Ceftizoxime" , and "Nystatin" for fungi

5. Conclusion

In this study, we successfully developed a novel eco-friendly film called PLA-CA-CUR-Ag NCs film using natural precursors derived from sukkari palm leaf, curcumin, and pomegranate peel. The combination of CA, CUR NPs, and Ag NPs on the PLA matrix was achieved through a solution-casting and ultrasonic irradiation method. The PLA-CA-CUR-Ag NCs film, among the four films prepared, exhibited unique properties with remarkable antimicrobial and antifungal efficacy. The incorporation of PLA, CA, CUR NPs, and Ag NPs resulted increased antibacterial activity against Bacillus subtilis, characterized by a significant 20 mm inhibition zone. Additionally, the film demonstrated antifungal activity against Candida albicans, showcasing a 14 mm inhibition zone diameter. These findings highlight the promising potential of the PLA-CA-CUR-Ag NCs film for various applications requiring efficient antimicrobial and antifungal properties.

Funding

No funding was received for conducting this study.

Conflict of interest

The authors declare no conflict of interest.

Ethical approval

There are no animal studies or human participants involved in this study. Therefore, the authors have no ethical approval to declare.

Informed consent

Informed consent was obtained from all individual participants included in the study.

6. References

[1] Claro, P. I. C., Neto, A. R. S., Bibbo, A. C. C., Mattoso, L. H. C., Bastos, M. S. R., Marconcini, J. M. Biodegradable blends with potential use in packaging: a comparison of PLA/chitosan and PLA/cellulose acetate films. Journal of Polymers and the Environment, 24(4), 363-371 (2016).

[2] Fischer, S., Thümmler, K., Volkert, B., Hettrich, K., Schmidt, I., Fischer, K. Properties and applications of cellulose acetate. Macromolecular symposia, 262, 89-96 (2008).

[3] Khoshnevisan, K., Maleki, H., Samadian, H., Shahsavari, S., Sarrafzadeh, M.H., Larijani, B., Dorkoosh, F. A., Haghpanah, V., Khorramizadeh, M. R., Cellulose acetate electrospun nanofibers for drug delivery systems: Applications and recent advances. Carbohydrate polymers, 198, 131-141 (2018).

[4] Liakos, I. L., D'autilia, F., Garzoni, A., Bonferoni, C., Scarpellini, A., Brunetti, V., Carzino, R., Bianchini, P., Pompa, P. P., Athanassiou, A. All natural cellulose acetate—Lemongrass essential oil antimicrobial nanocapsules. International journal of pharmaceutics, 510(2), 508-515 (2016).

[5] Liakos, I. L., Holban, A. M., Carzino, R., Lauciello, S., Grumezescu, A. M. Electrospun fiber pads of cellulose acetate and essential oils with antimicrobial activity. Nanomaterials, 7(4), 84 (2017).

[6] Gomaa, S. F., Madkour, T. M., Moghannem, S., El-Sherbiny, I. M. New polylactic acid/cellulose acetate-based antimicrobial interactive single dose nanofibrous wound dressing mats. International journal of biological macromolecules, 105, 1148-1160 (2017).

[7] Dairi, N., Ferfera-Harrar, H., Ramos, M., Garrigós, M. C. Cellulose acetate/AgNPs-organoclay and/or thymol nano-biocomposite films with combined antimicrobial/antioxidant properties for active food packaging use. International journal of biological macromolecules, 121, 508-523 (2019).

[8] Felgueiras, H. P., Teixeira, M. A., Tavares, T. D., Homem, N. C., Zille, A., Amorim, M. T. P. Antimicrobial action and clotting time of thin, hydrated poly (vinyl alcohol)/cellulose acetate films functionalized with LL37 for prospective wound-healing applications. Journal of Applied Polymer Science, 137(18), 48626 (2020).

[9] Lai, P., Roy, J. Antimicrobial and chemopreventive properties of herbs and spices. Current medicinal chemistry, 11(11), 1451-1460 (2004).

[10] Maheshwari, R. K., Singh, A. K., Gaddipati, J. P., Srimal, R. C. Multiple biological activities of curcumin: a short review. Life sciences, 78(18), 2081-2087 (2006).

[11] Hayakawa, H., Minaniya, Y., Ito, K., Yamamoto, Y., Fukuda, T. Difference of curcumin content in Curcuma longa L.(Zingiberaceae) caused by hybridization with other Curcuma species. American Journal of Plant Sciences, 2(02), 111 (2011).

[12] Anand, P., Nair, H. B., Sung, B., Kunnumakkara, A. B., Yadav, V. R., Tekmal, R. R., Aggarwal, B. B. Design of curcumin-loaded PLGA nanoparticles formulation with enhanced cellular uptake, and increased bioactivity in vitro and superior bioavailability in vivo. Biochemical Pharmacology, 79, 330-338 (2010).

[13] Sehim AE, Abdel-Ghafar RY, El-Nekeety AA: Antioxidant and antimicrobial efficiency of curcumin nanoparticles against pathogenic microorganisms. Egyptian Journal of Chemistry, 66(8), 383-392 (2023).

[14] Araujo, C. Leon, L. Biological activities of Curcuma longa L. Memórias do Instituto Oswaldo Cruz, 96(5), 723-728 (2001).

[15] Adamczak, A., Ożarowski, M., Karpiński, T. M., Curcumin, a Natural Antimicrobial Agent with Strain-Specific Activity. Pharmaceuticals (Basel), 13(7), 153 (2020).

[16] Anand, P., Kunnumakkara, A. B., Newman, R. A., Aggarwal, B. B., Bioavailability of curcumin: problems and promises. Molecular pharmaceutics, 4(6), 807-818 (2007).

[17] Varaprasad, K., Vimala, K., Ravindra, S., Reddy, N. N., Reddy, G., V. S., Raju, K. M. Fabrication of silver nanocomposite films

impregnated with curcumin for superior antibacterial applications. Journal of Materials Science: Materials in Medicine, 22(8), 1863-1872 (2011).
[18] Pandit, R. S., Gaikwad, S. C., Agarkar, G. A., Gade, A. K., Rai, M. Curcumin nanoparticles: physico-chemical fabrication and its in vitro efficacy against human pathogens. 3 Biotech, 5(6), 991-997 (2015).
[19] Goudarzi, M., Mir, N., Mousavi-Kamazani, M., Bagheri, S., Salavati-Niasari, M., Biosynthesis and characterization of silver nanoparticles prepared from two novel natural precursors by facile thermal decomposition methods. Scientific reports, 6, 32539 (2016).
[20] Ebrahima S, Abdelghanyb A, Ayada D, Abdelaala M: Role of Silver Nanoparticles on the Structure and Optical Properties of CS/PVP/AMOX Nanocomposites. Egyptian Journal of Chemistry, 67(2), 109-204 (2024).
[21] Brennan, S., C.N., Fhoghlú, B., Devitt, FJ, O′ mahony, D., Brabazon, A., Walsh. Silver nanoparticles and their orthopaedic applications. Bone Joint J, 97, 582-589 (2015).
[22] Azlin-Hasim, S., Cruz-Romero, M. C., Ghoshal, T., Morris, M. A., Cummins, E., Kerry, J. P. Application of silver nanodots for potential use in antimicrobial packaging applications. Innovative Food Science & Emerging Technologies, 27, 136-143 (2015).
[23] Tran, P.A., Hocking, D.M., O'Connor, A.J. In situ formation of antimicrobial silver nanoparticles and the impregnation of hydrophobic polycaprolactone matrix for antimicrobial medical device applications. Materials Science and Engineering: C, 47, 63-69 (2015).
[24] Yang, G., Wang, C., Hong, F., Yang, X., Cao, Z. Preparation and characterization of BC/PAM-AgNPs nanocomposites for antibacterial applications. Carbohydrate polymers, 115, 636-642 (2015).
[25] Xie, H., Xiong, N. N., Zhao, Y. Z., Wang, Y. H. Sintering Behavior and Electrical Property of Surface Treated Silver Nanoparticle for Electronic Application. in Key Engineering Materials. 645-646, 157-162 (2015).
[26] Doosthosseini, F., Behjat, A., Hashemizadeh, S., Torabi, N. Application of silver nanoparticles as an interfacial layer in cadmium sulfide quantum dot sensitized solar cells. Journal of Nanophotonics, 9(1), 093092 (2015).
[27] Liu, J., Cui, J., Vilela, F., He, J., Zeller, M., Hunterd, A. D., Xu, Z.In situ production of silver nanoparticles on an aldehyde-equipped conjugated porous polymer and subsequent heterogeneous reduction of aromatic nitro groups at room temperature. Chemical Communications, 51(61), 12197-12200 (2015).
[28] Frank, A. J., McEneny-King, A., Cathcarta, N., Kitaev, V. Homogeneously magnetically concentrated silver nanoparticles for uniform “hot spots” in surface enhanced Raman spectroscopy. RSC Advances, 5(90), 73919-73925 (2015).
[29] Karim, Z., Khan, M. J., Maskat, M. Y., Adnan, R. Immobilization of horseradish peroxidase on β-cyclodextrin-capped silver nanoparticles: Its future aspects in biosensor application. Preparative Biochemistry and Biotechnology, 46(4), 321-327 (2016).
[30] 30. Łopusiewicz, Ł., Jędra, F., Mizielińska, M. New poly (lactic acid) active packaging composite films incorporated with fungal melanin. Polymers, 10(4), 386 (2018).
[31] El-Gendy A, Abou-Zeid RE, Salama A, Diab MA-HA-R, El-Sakhawy M: TEMPO-oxidized cellulose nanofibers/polylactic acid/TiO2 as antibacterial bionanocomposite for active packaging. Egyptian Journal of Chemistry, 60(6), 1007-1014 (2017).
[32] Baran, E.H., Erbil, H.Y. Surface modification of 3D printed PLA objects by fused deposition modeling: a review. Colloids and interfaces, 3(2), 43 (2019).
[33] Scaffaro, R., Lopresti, F., Marino, A., Nostro, A. Antimicrobial additives for poly (lactic acid) materials and their applications: current state and perspectives. Applied microbiology and biotechnology, 102(18), 7739-7756 (2018).
[34] Al-Oqla, F.M., Sapuan, S. Natural fiber reinforced polymer composites in industrial applications: feasibility of date palm fibers for sustainable automotive industry. Journal of Cleaner Production, 66, 347-354 (2014).
[35] Alves, C., Ferrão, P.M.C., Silva, A.J., Reis, L.G., Freitas, M., Rodrigues, L.B., Alves, D.E. Ecodesign of automotive components making use of natural jute fiber composites. Journal of cleaner production, 18(4), 313-327 (2010).
[36] Sanjay, M.R., Madhu, P., Jawaid, M., Senthamaraikannan, P., Senthil, S., Pradeep, S. Characterization and properties of natural fiber polymer composites: A comprehensive review. Journal of Cleaner Production, 172, 566-581 (2018).
[37] Sanjay M.R., Siengchin, S., Parameswaranpillai, J., Jawaid, M., Pruncu, C. I., Khan, A. A comprehensive review of techniques for natural fibers as reinforcement in composites: Preparation, processing and characterization. Carbohydrate polymers, 207, 108-121 (2019).
[38] Bello, A., Isa, M. T., Aderemi, B. O., Mukhtar, B. Acetylation of cotton stalk for cellulose acetate production. American Scientific Research Journal for Engineering, Technology, and Sciences (ASRJETS), 15(1), 137-150 (2016).
[39] Niranjan, R., Kaushik, M., Prakash, J., Venkataprasanna, K.S., Christy, A. Pannerselvam, B., Venkatasubbu, G. D. Enhanced wound healing by PVA/Chitosan/Curcumin patches: In vitro and in vivo study. Colloids and Surfaces B: Biointerfaces, 182, 110339 (2019).
[40] Gunathilake, T. M. S. U., Ching, Y. C., Chuah, C. H., Abd Rahman, N., Nai-Shang, L. pH-responsive poly (lactic acid)/sodium carboxymethyl cellulose film for enhanced delivery of curcumin in vitro. Journal of Drug

Delivery Science and Technology, 58, 101787 (2020).
[41] Wikler, M., Cockerill, F. R., Bush, K., Dudley, M. N., Eliopoulos, G. M., Hardy, D. J., Hecht, D. W., Ferraro, M. J., Swenson, J., Hindler, J., Patel, J. B., Powell, M., Turnidge, J. D., Weinstein, M. P., Zimmer, B. L. Methods for dilution antimicrobial susceptibility tests for bacteria that grow aerobically: approved standard. CLSI (NCCLS), 26, M7-A7 (2006).
[42] Dong, Y., Yang, Y., Wei, Y., Gao, Y., Jiang, W., Wang, G., Wang, D. Facile synthetic nano-curcumin encapsulated Bio-fabricated nanoparticles induces ROS-mediated apoptosis and migration blocking of human lung cancer cells. Process Biochemistry, 95, 91-98 (2020).
[43] Raslan W, El-Salam A, El-Thalouth A, Kamal AK: Rendering of Some Properties of Cellulose Acetate Fabric through Treatment with Laser/TiO2 Nanoparticles in Alcoholic Media. Egyptian Journal of Chemistry, 67(1), 111-123 (2024).
[44] Bruni, S., De Luca, E., Guglielmi, V., Pozzi, F. Identification of natural dyes on laboratory-dyed wool and ancient wool, silk, and cotton fibers using attenuated total reflection (ATR) Fourier transform infrared (FT-IR) spectroscopy and Fourier transform Raman spectroscopy. Applied spectroscopy, 65(9), 1017-1023 (2011).
[45] Casanova-González, E., García-Bucio, A., Ruvalcaba-Sil, J. L., Santos-Vasquez, V., Esquivel, B., Roldán, M. L., Domingo, C. Silver Nanoparticles for SERS Identification of Dyes. MRS Online Proceedings Library, 1374(1), 263-274 (2012).
[46] Hosseinpour-Mashkani, S.M., Ramezani, M. Silver and silver oxide nanoparticles: Synthesis and characterization by thermal decomposition. Materials Letters, 130, 259-262 (2014).
[47] Khan, A.U., Khan, M., Khan, M.M. Antifungal and antibacterial assay by silver nanoparticles synthesized from aqueous leaf extract of Trigonella foenum-graecum. BioNanoScience, 9(3), 597-602 (2019).
[48] Battisti, R., Hafemann, E., Claumann, C. A., Machado, R. A. F., Marangoni, C. Synthesis and characterization of cellulose acetate from royal palm tree agroindustrial waste. Polymer Engineering & Science, 59(5), 891-898 (2019).
[49] Terinte, N., Ibbett, R., Schuster, K.C. Overview on native cellulose and microcrystalline cellulose I structure studied by X-ray diffraction (WAXD): Comparison between measurement techniques. Lenzinger Berichte, 89(1), 118-131 (2011).
[50] Wang, N., Yu, J., Ma, X. Preparation and characterization of compatible thermoplastic dry starch/poly (lactic acid). Polymer Composites, 29(5), 551-559 (2008).
[51] Shameli, K., Bin Ahmad, M., Yunus, W. M. Z. W., Ibrahim, N. A., Abdul Rahman, R., Jokar, M., Darroudi, M. Silver/poly (lactic acid) nanocomposites: preparation, characterization, and antibacterial activity. International journal of nanomedicine, 5, 573-579 (2010).
[52] 52. Gong, X., Pan, L., Tang, C. Y., Chen, L., Hao, Z., Law, W.-C., Wang, X., Tsui, C. P., Wu, C. Preparation, optical and thermal properties of CdSe–ZnS/poly (lactic acid)(PLA) nanocomposites. Composites Part B: Engineering, 66, 494-499 (2014).
[53] Fu, Y., Wu, G., Bian, X., Zeng, J., Weng, Y. Biodegradation behavior of poly (butylene adipate-co-terephthalate)(PBAT), poly (lactic acid)(PLA), and their blend under soil conditions. Molecules, 25(17), 3946 (2020).
[54] Al-Itry, R., Lamnawar, K., Maazouz, A. Rheological, morphological, and interfacial properties of compatibilized PLA/PBAT blends. Rheologica acta, 53(7), 501-517 (2014).
[55] Katowah, D. F., Saleh, S. M., Alqarni, S. A., Ali, R., Mohammed, G. I., Hussein, M. A. Network structure-based decorated CPA@ CuO hybrid nanocomposite for methyl orange environmental remediation. Scientific Reports, 11(1), 5056 (2021).
[56] Katowah, D. F., Mohammed, G. I., Al-Eryani, D. A., Osman, O. I., Sobahi, T. R., Hussein, M. A. Fabrication of conductive cross-linked polyaniline/G-MWCNTS core-shell nanocomposite: A selective sensor for trace determination of chlorophenol in water samples. Polymers for Advanced Technologies, 31(11), 2615-2631 (2020).
[57] Katowah, D. F., Hussein, M. A., Alam, M.M., Ismail, S. H., Osman, O.I., Sobahi, T.R., Asiri, A. M., Ahmed, J., Rahman, M. M. Designed network of ternary core-shell PPCOT/$NiFe_2O_4$/C-SWCNTs nanocomposites. A Selective Fe^{3+} ionic sensor. Journal of Alloys and Compounds, 834, 155020 (2020).
[58] Katowah, D. F., Mohammed, G. I., Al-Eryani, D. A., Sobahi, T. R., Hussei, M. A. Rapid and sensitive electrochemical sensor of cross-linked polyaniline/oxidized carbon nanomaterials core-shell nanocomposites for determination of 2, 4-dichlorophenol. PloS one, 15(6), e0234815 (2020).